Journal of Quantitative Spectroscopy & Radiative Transfer 235 (2019) 209–216

Contents lists available at ScienceDirect

Journal of Quantitative Spectroscopy & Radiative Transfer

journal homepage: www.elsevier.com/locate/jqsrt

CH_4 broadening and shifting coefficients in the Fermi triad of $^{12}C^{16}O_2$ in the 2 μm region

A.V. Domanskaya[a,*], R.E. Asfin[b], A.A. Kyuberis[c], V. Ebert[a,*]

[a] Physikalisch-Technische Bundesanstalt (PTB), Bundesallee 100, 38116 Braunschweig, Lower Saxony, Germany
[b] Faculty of Physics, St. Petersburg State University, Peterhof, St. Petersburg 198504, Russian Federation
[c] Institute of Applied Physics, Russian Academy of Science, Ulyanov Street 46, Nizhny Novgorod 603950, Russian Federation

ARTICLE INFO

Article history:
Received 27 May 2019
Revised 3 July 2019
Accepted 3 July 2019
Available online 4 July 2019

Keywords:
Pressure broadening
Pressure shifting
Fermi triad
Carbon dioxide
Methane
Infrared
Hydrocarbon
Gas
FTIR

ABSTRACT

Novel experimental values of collisional broadening and shifting coefficients for the Fermi triad of CO_2 in mixture with methane at 296.0(2) K were determined from high resolution FTIR measurements. An empirical function for the broadening coefficients is obtained: $\gamma_n(J') = 0.0762(7) + 0.00320(4) \cdot \exp(-0.039(3) \cdot J')$ /cm^{-1}/atm, here J' refers to the final state, $n = 1, 2, 3$ labels the Fermi components. Expanded uncertainties (2σ) for 38 out of 55 reported values are smaller than 0.5%. The absolute values of shift coefficients are about ten times smaller than the broadening, and the relative uncertainty is larger (4–5%).

1. Introduction

CO_2 and CH_4 are gases of interest for atmospheric chemistry, combustion [1], biogas [2] and biomethane [3]. Consequently, there has been increased need in their disposal, removal and utilization as well as understanding of their influence in the atmosphere. The reaction between CO_2 and CH_4 to produce CO and H_2 is an essential step for CO_2 removal from methane enriched mixtures and several other processes [4,5].

Gas monitoring during a technological process is often done by spectroscopic measuring techniques [1,6], such as TDLAS [6,7], which allow high speed gas analysis by scanning small spectral intervals rapidly. Spectroscopy-based techniques often require an accurate prior knowledge of molecular parameters, such as line strengths, transition wavenumbers and collisional line parameters. The latter is the focus of the current article.

The spectrum of methane has a distinctive structure: vibrational bands cluster in so-called polyads, leaving absorption-free transparency windows. Carbon dioxide, in turn, absorbs in the gaps between methane polyads (see Fig. 1). This is very fortunate, because the spectral signatures of the two species are then easier to separate from each other, unlike the HCl–CH_4 system, for example, where the absorption bands strongly overlap [8,9]. Another fortunate coincidence is that the lines of water combination bands are substantially higher in wavenumber than the CO_2 bands of interest.

The CO_2 Fermi triad consists of three Σ-symmetry bands, $4\nu_2 + \nu_3$ at 4853.6231494(56) cm^{-1}, $\nu_1 + 2\nu_2 + \nu_3$ at 4977.8346548(63) cm^{-1} and $2\nu_1 + \nu_3$ at 5099.6601778(56) cm^{-1} ($20^013 \leftarrow 00^001$, $20^012 \leftarrow 00^001$ and $20^011 \leftarrow 00^001$[1] in the notation scheme used in the HITRAN database [10]) [11,12]. Even though the region of the Fermi triad is little affected by methane absorption, the spectrum remains quite crowded (see Fig. 2). At room temperature the hot transitions $21^11n \leftarrow 01^11$ ($n = 1...3$) are clearly visible. The interval between the lines of the hot transitions is two times smaller than in the triad, the intensity is about an order of magnitude less [11]. In samples with natural isotopic abundance the bands of $^{13}C^{16}O_2$ have a noticeable contribution as well.

* Corresponding authors.
E-mail addresses: alexandra.luettschwager@ptb.de, domav@yandex.ru (A.V. Domanskaya), volker.ebert@ptb.de (V. Ebert).

[1] Notation of a vibrational energy level used in HITRAN is (ν_1, ν_2^l, ν_3, n), where ν_i is the quantum number of corresponding vibrational mode, l is the value of l-type doubling, and n labels the Fermi components.

https://doi.org/10.1016/j.jqsrt.2019.07.004
0022-4073/

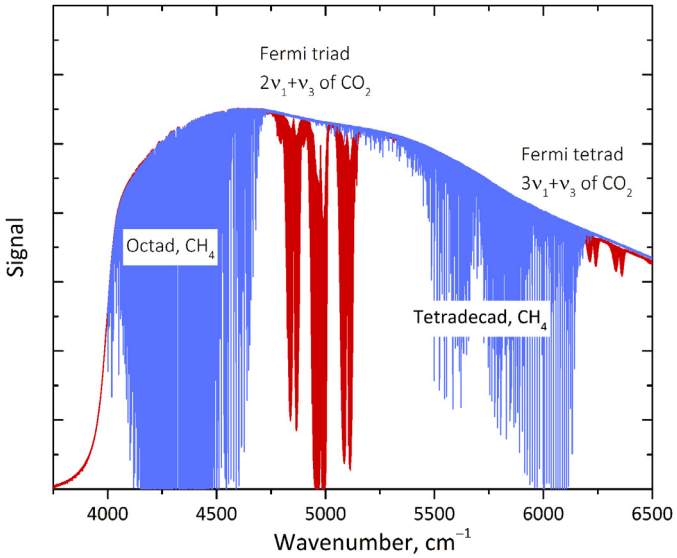

Fig. 1. Overview of CH_4 and CO_2 absorption features in the near infrared region.

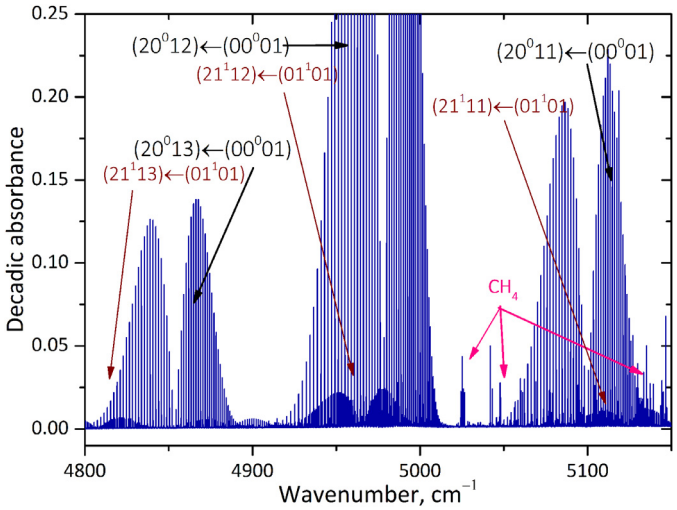

Fig. 2. Experimental spectrum of CO_2-CH_4 mixture in the region of Fermi triad at room temperature. Total pressure is 116.3 hPa with 5.5 hPa of CO_2 (natural abundance), absorption path is 3.2 m.

Several studies report the collisional line parameters for different CO_2 bands. Several datasets of the CO_2 broadening by CO_2 (self), N_2, O_2 or air were carefully analyzed in the works by Gamache and Lamouroux [13] and Gamache et al. [14] Studies of the Fermi triad were mostly focused on two lower frequency components, $20^01n\leftarrow00^001$ with $n=3$ and 2, because these two are less affected by absorption of other atmospheric species. An exception are the FTIR broadband studies of Toth et al. [12,15] which form the basis for the HITRAN [10] entries for the triad.

As far as we know, only one article is dedicated to the CO_2–CH_4 system. Bürkle et al. [16] studied a set of lines for combustion-relevant molecules by TDLAS, including one line of CO_2 (R_{18}e of $20^012\leftarrow00^0{\cdot}011$ band). Broadening and shifting coefficients by CO_2, N_2, O_2, air, C_2H_2 and, finally, CH_4 are reported.

In the current work, done in collaboration between PTB (experiment) and Saint Petersburg State University (spectral data analysis), we report an extensive set of broadening and shifting coefficients of CO_2 interacting with methane for all three components of Fermi triad. Part of the results is intended for use for biomethane analysis [3].

2. Experiment and analysis

2.1. Measurement

The absorption spectra were recorded with a Bruker 125 HR FTIR instrument of the EUMETRISPEC [17] facility at PTB. The spectrometer was equipped with a CaF_2/Si beamsplitter, a tungsten lamp as a light source and an InGaAs detector. The spectral resolution was set to 0.005 cm^{-1}. The apodisation function was Boxcar. The spectra are an average of about 1000 scans except for the 102.2, 116.3 and 209.8 hPa measurements, which ran over a weekend with ~2400 accumulated scans (see Table 1). The sample cell was a multipass White cell with adjustable absorption path set to 3.2 m (base length is 40 cm). The cell was temperature stabilized by circulating liquid coolant (water).

High purity CH_4 (5.5, Linde) and CO_2 (4.5, Linde) were used as supplied. First, a few hPa of pure CO_2 was admitted to the cell, and then CH_4 was added in steps of about 25 hPa (see Table 1 for more details). Spectra were measured after every dilution step. The strongest lines of the water combination bands, situated in the low wavenumber region of the CO_2 Tetradecad, did not exceed $5\cdot10^{-3}$ decimal absorbance level. High total pressures cause the lines to overlap and increase methane absorption, which complicates the modeling, small pressures result in small collisional widths which are more difficult to separate from the contributions of the instrument function (ILS) and the Doppler width. The choice of the pressures was a compromise between these factors. Two series of measurements (with 2 and 5.5 hPa CO_2 partial pressure) were performed.

The pressures of the pure gas and the mixture were measured by two ceramic capacitance diaphragm pressure gauges (upper limit of 13 and 1333 hPa), calibrated with reference to the German national standard. The readings were logged with an interval of 1 min. For the most samples, the pressure variation during measurements was below 0.04 hPa, which is one order of magnitude less than the accuracy of the calibration (~0.3 hPa). Hence the total pressure uncertainty was almost entirely determined by the latter.

The temperature was monitored by two calibrated PT-100 temperature sensors, attached to the top and the bottom of the cell's body. The calibration showed that the difference between the reference values and the actual measurements remains within $3\cdot10^{-2}$ K, which exceeds the absolute temperature accuracy of $2\cdot10^{-2}$ K, stated by the manufacturer. During the measurements the temperature remained stable typically within $\sim5\cdot10^{-2}$ K, but there was a persistent gradient of 0.35 K along the cell. Therefore, we take an average of the two sensors as a measure of the gas temperature, with the uncertainty accounting for the instrument's calibration accuracy, variation during the measurement and a half of the gradient. It results in a value of 0.2 K for the most measurements (Table 1).

It is worth noting, that the measurement at 102.2 hPa of the series with 2 hPa of CO_2 is rather an exception. There, the stability of pressure and temperature was worse than in any other sample, which is reflected in higher uncertainties (Table 1). It was found afterwards, that there were oscillations in the temperature in the lab, which were compensated by the thermostation system only with a delay.

2.2. Data treatment

The transmission spectra were evaluated using the capabilities of Origin 9.0 software (non-linear optimization algorithm, as well as build-in functions). A LabTalk script, developed in State University of St. Petersburg, automated the analysis. The same method was used in Ref. 18. It goes as following: a micro-window 60

Table 1
Parameters of the CO_2–CH_4 mixtures, used in the experiments. Here p is the total pressure of the mixture in hPa, and T is the temperature in Kelvin. Duration is the time of spectroscopic measurement. Expanded uncertainties (2σ) are shown in parentheses.

	Series 1: 2.0 hPa CO_2			Series 2: 5.5 hPa CO_2		
CO_2+CH_4	p, hPa	T, K	Duration, hh:mm	p, hPa	T, K	Duration, hh:mm
1	102.2(9)	296(2)	65:58	116.3(2)	295.9(2)	63:39
2	127.3(2)	295.8(2)	24:48	140.9(2)	295.9(2)	29:10
3	152.2(3)	295.8(2)	24:49	164.7(3)	296.0(2)	39:54
4	177.0(3)	295.8(2)	24:49	185.3(3)	295.9(2)	29:07
5	202.2(3)	295.9(2)	22:39	209.8(4)	295.9(2)	63:39

FWHM wide is sequentially centered on a CO_2 line of the triad, and absorption features of both, methane and CO_2, falling within this interval, are simultaneously fitted with Voigt profiles. Starting FWHM was determined from a quick fit of the central line. The number of sixty was chosen somewhat arbitrary, but it is certainly large enough for the absorption of the central line wings to become weaker than the noise level. The Doppler half width ($w_D = \frac{\nu}{c}\sqrt{\frac{2\ln 2 \cdot kT}{m}}$), which is about $5 \cdot 10^{-3}$ cm^{-1} in our case, was calculated for every CO_2 line. The baseline correction was done in two steps: first the baseline in a form of first order polynomial was subtracted for every band, and then a constant offset for each micro-window was taken into account during the fitting process. It is worth noting, that this offset was found to be within the noise margin in most cases.

Initial line positions and intensities were taken from HITRAN 2016 [10]. In the interval 4775–5150 cm^{-1} HITRAN 2016 yields over 15,000 lines for the main CO_2 isotopologue alone. The lines of CO_2 with intensities below $5 \cdot 10^{-25}$ $cm^{-1}/(molec \cdot cm^{-2})$ were not fitted because their contributions to the spectral profile are below the noise level. For the CH_4 lines, the cut-off rule was set to $5 \cdot 10^{-27}$ $cm^{-1}/(molec \cdot cm^{-2})$ since there is about a hundred times more methane in the samples than CO_2.

One can see from Fig. 3 that even the lines with high J quantum number (= small collisional width) are well described by the Voigt profile. The lower panel of Fig. 3 is a close–up of the residuals, which remain featureless at least within 1% of peak intensity.

The stability of the CO_2 amount during the measurements was verified. An intensity increase of $2.1(3) \cdot 10^{-2}$%/hPa was detected for Series 1. It was probably caused by co–adding adsorbed CO_2 from the gas lines and cell walls during dilution of mixtures. The changes in Series 2 were marginal – only $0.3(2) \cdot 10^{-2}$%/hPa. The effect of the absorber gas variation Δp on the collision widths depends on the product of Δp ($4.2(7) \cdot 10^{-2}$ and $1.6(10) \cdot 10^{-2}$ hPa for Series 1 and 2 respectively) and the difference between self- and foreign- broadening coefficients. The maximum difference $|\gamma_{CO2} - \gamma_{CH4}|$[2] is about 0.01 cm^{-1}/atm ($0.97 \cdot 10^{-5}$ cm^{-1}/hPa). Therefore, the upper limit for the width change is less than $5 \cdot 10^{-7}$ cm^{-1}, which is far beyond our detection capabilities. The absolute values of the shifting coefficients are typically smaller than broadening coefficients, hence the effect on shifts due to the CO_2 variation within a series is even smaller.

Since the CO_2 partial pressure changed insignificantly within a series, a simplified treatment can be applied. The perturber broadening/shifting coefficients are determined separately for different series from the slope of linear regressions for widths/line positions as a function of total pressure. The intercepts of such regressions contain the instrumental and absorber specific parameters: they are a combination of self-broadening and width of the instrument function for the widths (~resolution), or the sum of vacuum wavenumbers with self-shifting. A cross-check of the validity of such an approach is the agreement between the perturber-related values (slopes) from different series. If there is a congruence, then the perturber-specific line parameters can be averaged over the series, and no additional data on self-shifting and broadening is necessary as well as a detailed knowledge of the absorber's partial pressure.

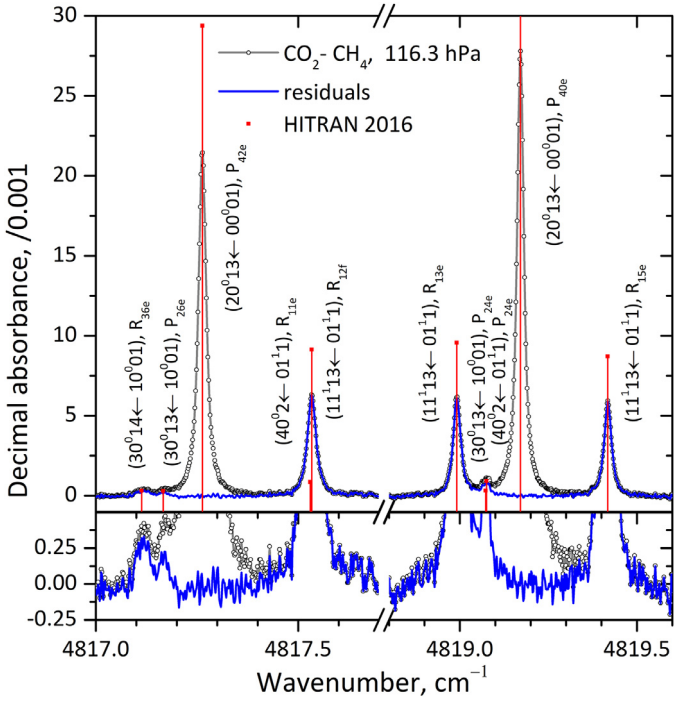

Fig. 3. Example of the fit. The blue solid line represents the residual spectrum after the Voight shaped lines of the ($20^0 13 \leftarrow 00^0 01$) CO_2 band were subtracted. Labeled bands of hot and combination bands were accounted in the fit. The lower panel shows a close-up of the residuals.

In this study we use the generalized linear regression analysis, based on the York algorithm by York et Evensen [19] accounting for uncertainties on both axes. For the averaging we use weights ω_k based on the variances $V(X_k)$:

$$\omega_k = \frac{\frac{1}{V(X_k)}}{\sum_{i=1}^{N} \frac{1}{V(X_i)}} \text{ with } V(X_k) = \sigma^2(X_k). \quad (1)$$

Here X_k is an individual value of shift δ or broadening γ, $\sigma(X_k)$ is the uncertainty of this value and N is the number of the values being averaged.

The uncertainty of the average value X is, in turn,

$$\Delta X = \sqrt{\sum_{i=1}^{N} \frac{1}{V(X_i)}}. \quad (2)$$

[2] Data on self-broadening was taken from Ref. [12].

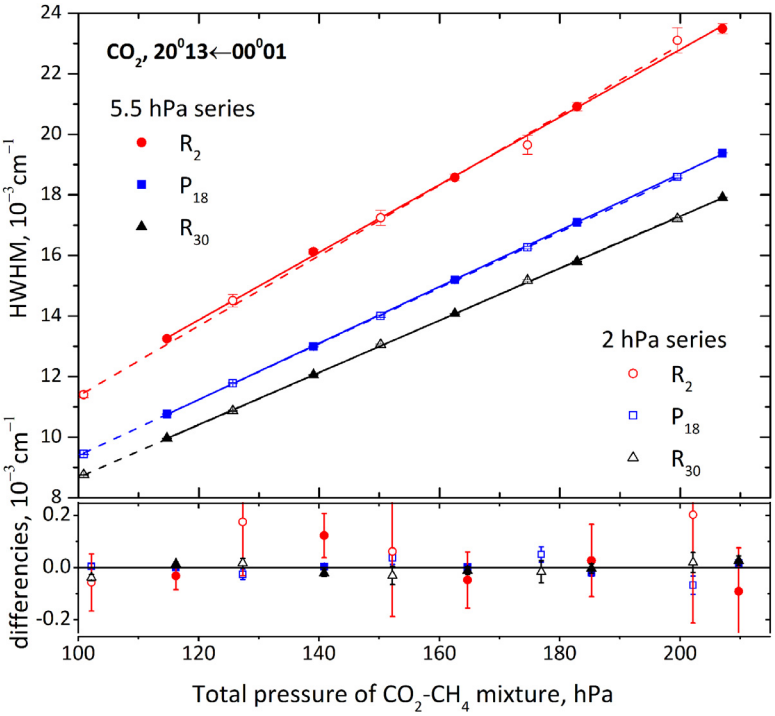

Fig. 4. An example of the linear fits of widths as function of pressure for three different lines of the ($20^0 13 \leftarrow 00^0 01$) band of CO_2 perturbed by CH_4. The plotted uncertainties correspond to 1σ of the Voigt fit (see text).

3. Results and discussion

3.1. Broadening

Fig. 4 shows some typical examples of the linear fits of the experimental half-widths. One can see that for higher J the agreement between the series of measurements is excellent, with deviations from linearity less than $0.5 \cdot 10^{-4}$ cm^{-1} (an order of magnitude smaller that the nominal spectral resolution). For the broad and weak lines near the band center the deviations grow larger. Uncertainties of the 2.0 hPa series exceed those of 5.5 hPa series, but there is good agreement even with 1σ uncertainty limit.

Broadening coefficients are depicted in Fig. 5 and listed in Table 2. They coincide for all three bands of the triad for most lines. A few, though, noticeably deviate from the general trend. Most of them belong to the higher frequency $20^0 11 \leftarrow 00^0 01$ component (orange diamonds in Fig. 5), which is the most affected by methane absorption of Tetradecad. As a result, a few systematic deviations appear.

Following the approach of Toth et al., [12,15] who also did not register any significant difference between the components of Fermi triad in pure CO_2 and mixtures with air, we calculated a weighted average for the values for different bands for every line index m[3] (solid line with squares in Fig. 5).

We evaluated the metrological compatibility [20] f between the average broadening coefficients and the individual values for the Fermi components. The international vocabulary of metrology [20] defines the denominator of comparability f as "some chosen multiple of the standard measurement uncertainty of that difference", so we took the liberty to use $\sqrt{2}$ as a scaling factor:

$$f = \frac{1}{\sqrt{2}} \cdot \frac{X_1 - X_2}{\sqrt{\Delta X_1{}^2 + \Delta X_2{}^2}}. \quad (4)$$

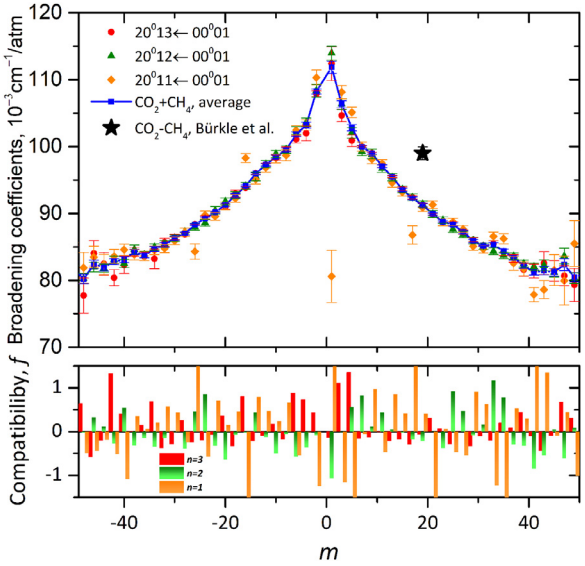

Fig. 5. CH_4 broadening coefficients of Fermi triad. Red circles, green triangles and orange diamonds correspond to the values of $20^0 13 \leftarrow 00^0 01$, $20^0 12 \leftarrow 00^0 01$ and $20^0 11 \leftarrow 00^0 01$ components, respectively. Blue curve with rectangles is the weighted average. Black star represents the data from Ref. [16]. Lower panel shows the compatibility value f (see text).

Then the compatibility criterion $|f| \leq 1$ (two values X_1 and X_2 are compatible) is close to the traditional concept of "staying within the error". As one can see in Fig. 5, most of the f-values satisfy the compatibility criterion with 2σ uncertainty level.

The broadening coefficients from different branches but with the same J[4] are almost identical (Fig. 6). The same is true for self- and air broadening [21]. Exceptions in all cases are the lines with

[3] $m = -J''$ for P-branch and $J''+1$ for R-branch. J'' refers to the initial state.

[4] J' is the rotational quantum number of the final state.

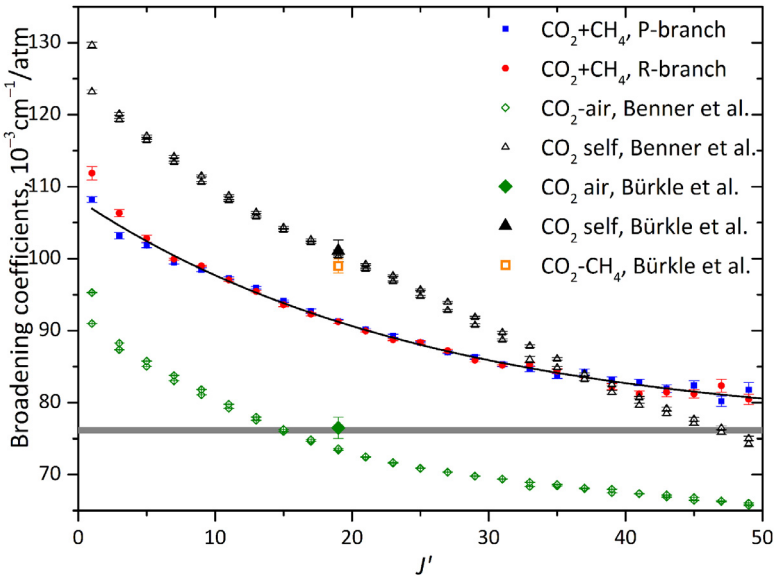

Fig. 6. Broadening coefficients of Fermi triad. Broadening coefficients for both branches are plotted as function of J' of the final state (filled rectangles and circles). Data for CO_2 self- (triangles) and air-shifting (diamonds) coefficients for $20^013 \leftarrow 00^001$ is taken from Ref. [21]. The data for $R_{18}e$ for the same band, taken from Ref. [16], is marked by open rectangle (-CH_4), filled diamond (-air) and filled triangle (-self). The thick horizontal line marks the asymptotic value for CO_2–CH_4 broadening coefficients.

small $J' = 1$ or 2, where the molecules are most susceptible to intermolecular interactions. The general trend for the CO_2–CH_4 system follows a simple exponential function (shown in Fig. 6 by a thin solid line):

$$\gamma(J') = 0.0762(7) + 0.00320(4) \cdot \exp(-0.039(3) \cdot J')/\mathrm{cm}^{-1}/\mathrm{atm} \quad (5)$$

The coefficient of determination R^2 for this fit is 0.991. This empirical function (5) has a physical asymptotote of 0.0762(7) cm^{-1}/atm (shown in Fig. 6 by a thick horizontal line), originating from vibrational motion [13]. The function (5) can be used for extrapolating the broadening coefficients to high J, unlike some of the multiparameter functions similar to the one, proposed in Ref. [12], which can start to grow or become negative at high J.

The only value of CO_2–CH_4 broadening known to us from the literature was reported in Ref. [16] for $R_{18}e$ of $20^012 \leftarrow 00^0011$. It is significantly larger than our value (Fig. 5). The f-value (Eq. (4)) exceeds five if we take our value for the middle band and the value from Ref. [16]. f drops to five, if we double the uncertainty, given in Ref. [16], assuming that the original table contains 1σ values (there is no clear indication on that in the text). The measurements in Ref. [16] were done in ten times broader interval of pressures than in our study. There is always a risk for broad intervals, that the linearity of the linewidths will not be maintained. It might be caused by non-linearity of the equation of state, by collapse of the hyperfine structure or influence of the line mixing, for example. One can see in Figs. 6 and 7 of Ref. [16], that the deviations of the line widths and line positions from the linear fit indeed show a systematic behavior. However, the effect of non-linearity cannot explain the observed mismatch in full, especially since this effect has typically an opposite sign – the values of the broadening coefficients are decreasing if the pressure interval is increasing and non-linearity is neglected. Apart from that we fail to point a possible uncertainty source, which might have caused the difference.

We compared other measurements from Ref. [16] for self- and air- broadening with the results of Toth et al., [12,15] and a recent broadband study of Benner et al. [21] (see Fig. 6). The agreement is perfect for the self-broadening, but the value for air-broadening overshoots the data from Refs. [15,21]: f is equal 2.7 for Bürkle-Benner, and 1.8 for Bürkle–Toth pairs.

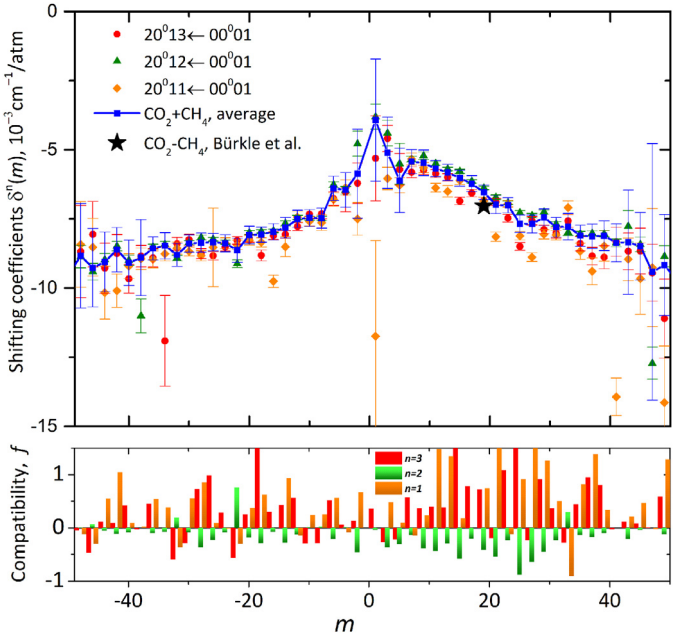

Fig. 7. CH_4-shifting coefficients of Fermi triad. The data points in the upper panel have the same labels as in Fig. 5. The lower panel shows the compatibility value f (see text).

3.2. Shifting

Since CO_2 and CH_4 are non-polar molecules, their interaction is weak, resulting in rather small shifting of the lines. All shifting coefficients are bathochromic (negative) and small, their absolute value remaining under $10 \cdot 10^{-3}$ cm^{-1}/atm (see Table 3). To compare, the absolute values of the shifting coefficients for the first overtone of HCl, perturbed even by hydrogen, are 1.5 times larger [8]. The HCl–CH_4 shifts are more than three times larger for high J [8], even though the shifts depend on the vibrational excitation [22], and the latter is smaller for the HCl overtone than for Fermi triad.

Table 2
Pressure broadening γ^n (in 10^{-3} cm^{-1}/atm) of carbon dioxide lines of ($20^0 01n \leftarrow 00^0 01$) bands ($n = 1, 2, 3$) in mixtures with methane at 296.0(2) K. Expanded uncertainties (2Δ) are shown in parentheses. Here Δ is the standard error of the weighted mean.

m	γ^n, 10^{-3} cm^{-1}/atm			γ, 10^{-3} cm^{-1}/atm
	$n=3$	$n=2$	$n=1$	Weighted mean
−56	80(10)	78(2)	90(10)	78(2)
−54	95(4)	80(2)	87(6)	83(2)
−52	82(5)	82(1)	90(4)	82(1)
−50	90(5)	81(1)	83(3)	82(1)
−48	78(3)	80.2(8)	82(2)	80.2(7)
−46	84(2)	82.0(7)	84(2)	82.4(6)
−44	83(2)	81.8(6)	82(2)	82.0(5)
−42	80(1)	83.1(6)	84(1)	82.8(4)
−40	82(1)	82.5(6)	84.6(8)	83.1(5)
−38	84.3(6)	84.6(7)	83.8(8)	84.3(4)
−36	83.6(6)	83.8(5)	83.7(7)	83.7(3)
−34	83(1)	85.0(5)	84.5(6)	84.7(4)
−32	85.7(6)	85.4(5)	84.8(6)	85.3(3)
−30	86.5(4)	86.3(5)	85.9(6)	86.3(3)
−28	86.9(3)	87.3(5)	87.2(6)	87.0(2)
−26	88.4(1)	88.0(5)	84(1)	88.3(1)
−24	89.4(3)	88.6(5)	89.8(6)	89.3(2)
−22	90.2(1)	90.5(6)	89.6(6)	90.2(1)
−20	91.0(4)	91.8(5)	91.1(6)	91.3(3)
−18	93.0(5)	92.7(5)	92.3(6)	92.7(3)
−16	93.9(2)	94.1(5)	98.3(7)	94.1(2)
−14	96.0(2)	95.5(7)	95.1(7)	96.0(2)
−12	97.3(2)	97.4(5)	96.8(6)	97.3(2)
−10	98.4(4)	98.9(5)	98.2(6)	98.5(3)
−8	99.6(3)	99.6(6)	98.7(8)	99.5(3)
−6	101.1(5)	102.4(6)	102.5(7)	101.9(3)
−4	102(1)	103.6(6)	103.2(8)	103.2(4)
−2	107.9(5)	108(1)	110(1)	108.2(4)
1	112(3)	114(1)	81(4)	111.9(9)
3	104.6(9)	106.3(8)	108(1)	106.3(5)
5	100.9(9)	102.1(8)	105.1(8)	102.8(5)
7	100.0(2)	99.2(6)	100.0(7)	100.0(2)
9	99.0(1)	98.9(7)	98.1(7)	99.0(1)
11	97.1(2)	96.7(5)	97.5(6)	97.1(2)
13	95.5(2)	95.4(5)	94.6(7)	95.5(2)
15	93.7(3)	93.6(5)	93.2(6)	93.6(2)
17	92.4(2)	92.4(5)	87(1)	92.3(2)
19	91.3(3)	91.4(5)	90.9(6)	91.2(2)
21	89.9(1)	89.9(5)	91.3(6)	89.9(1)
23	88.7(1)	89.0(5)	88.7(5)	88.7(1)
25	88.5(3)	87.6(5)	88.8(6)	88.4(2)
27	87.2(3)	86.9(5)	87.7(5)	87.2(2)
29	86.1(3)	86.0(5)	85.1(6)	85.9(2)
31	85.2(1)	85.1(5)	84.7(6)	85.2(1)
33	85.5(5)	84.3(5)	86.6(6)	85.3(3)
35	84.2(5)	83.7(5)	86.2(7)	84.4(3)
37	83.3(6)	83.6(5)	83(1)	83.4(3)
39	81.6(9)	82.5(5)	82(1)	82.2(4)
41	81(1)	82.1(5)	78(1)	81.2(4)
43	83(2)	82.3(8)	79(1)	81.5(6)
45	81(2)	81.2(6)	82(2)	81.2(6)
47	81(2)	84(1)	80(4)	82.4(9)
49	79(2)	80.3(8)	86(3)	80.5(7)
51	79(3)	80.0(9)		80.0(8)
53	73(4)	82(3)	80(10)	78(2)

Table 3
Pressure shifting δ^n (in 10^{-3} cm^{-1}/atm) of carbon dioxide lines of ($20^0 01n \leftarrow 00^0 01$) bands ($n = 1, 2, 3$) in mixtures with methane at 296.0(2) K.

m	δ^n, 10^{-3} cm^{-1}/atm			δ, 10^{-3} cm^{-1}/atm
	$n=3$	$n=2$	$n=1$	Weighted mean*
−56		−7(1)	−6(9)	
−54		−9(1)		−9(5)
−52	−7(4)	−9.2(7)	−8(3)	−9(3)
−50		−9.5(6)	−10(2)	−10(3)
−48	−9(2)	−8.9(4)	−8(2)	−9(2)
−46	−8(1)	−9.4(3)	−9(1)	−9(1)
−44	−9.3(9)	−9.0(2)	−10(1)	−9(1)
−42	−8.7(7)	−8.5(2)	−10.1(6)	−8.6(8)
−40	−9.7(5)	−9.0(2)	−9.2(4)	−9.1(8)
−38	−8.9(4)		−8.9(4)	−9(1)
−36	−8.9(3)	−8.51(9)	−9.0(3)	−8.6(4)
−34		−8.4(1)	−8.8(3)	−8.5(5)
−32	−8.4(2)	−8.9(1)	−8.6(2)	−8.8(4)
−30	−8.2(2)	−8.36(7)	−8.7(2)	−8.4(3)
−28	−8.8(2)	−8.17(8)	−8.8(2)	−8.4(3)
−26	−8.8(2)	−8.23(7)	−9(1)	−8.3(3)
−24	−8.5(1)	−8.35(7)	−8.4(2)	−8.4(3)
−22	−8.3(1)	−9.1(1)	−8.4(2)	−8.6(4)
−20	−8.2(1)	−8.00(8)	−8.3(2)	−8.1(3)
−18	−8.8(2)	−7.95(6)	−8.3(2)	−8.1(3)
−16	−8.1(1)	−7.93(7)		−8.0(3)
−14	−8.1(1)	−7.66(9)	−8.5(4)	−7.8(4)
−12	−7.8(1)	−7.44(7)	−7.4(2)	−7.5(3)
−10	−7.3(2)	−7.47(7)	−7.6(2)	−7.5(3)
−8	−7.3(2)	−7.49(8)	−7.6(3)	−7.5(4)
−6	−6.8(2)	−6.3(1)	−6.8(2)	−6.4(4)
−4	−6.5(7)	−6.5(1)	−6.4(3)	−6.5(6)
−2	−6.2(7)	−4.8(4)	−7.5(6)	−6(2)
1	−5(2)	−3.8(5)		−4(2)
3	−4.6(5)	−4.4(5)	−6.0(4)	−5(1)
5	−5.7(6)	−5.5(7)	−6.3(3)	−6(1)
7	−5.8(2)	−5.3(1)	−5.3(2)	−5.4(4)
9	−5.7(2)	−5.2(1)	−5.6(2)	−5.5(5)
11	−5.9(1)	−5.50(7)	−6.4(2)	−5.7(3)
13	−6.0(1)	−5.70(7)	−6.5(2)	−5.8(3)
15	−6.9(1)	−5.78(7)	−6.1(2)	−6.0(3)
17	−6.6(1)	−6.14(6)		−6.2(3)
19	−6.8(1)	−6.38(7)	−6.9(1)	−6.5(3)
21	−6.9(1)	−6.72(9)	−8.1(2)	−7.0(3)
23	−7.5(1)	−6.92(7)	−7.0(1)	−7.0(3)
25	−8.5(1)	−7.28(8)	−8.1(1)	−7.7(3)
27	−7.6(1)	−7.38(8)	−8.9(2)	−7.7(3)
29	−7.9(2)	−7.25(7)	−8.1(2)	−7.4(3)
31	−8.0(2)	−7.68(9)	−8.1(2)	−7.8(4)
33	−7.6(2)	−8.0(1)	−7.1(2)	−7.8(5)
35	−8.4(3)	−8.04(8)	−8.7(3)	−8.1(4)
37	−8.8(3)	−8.02(9)	−9.4(5)	−8.1(4)
39	−8.9(4)	−8.0(1)	−8.5(5)	−8.1(5)
41	−8.3(5)	−8.4(1)		−8.4(7)
43	−8.7(7)	−7.8(6)	−9.0(8)	−8.3(2)
45	−8.7(8)	−8.4(3)	−10(1)	−9(1)
47	−10(1)		−9(2)	−9(5)
49	−11(1)	−8.9(4)	−14(2)	−9(2)
51	−10(2)	−9.7(5)		−9(2)
53	−8(3)	−8.8(6)		

* Uncertainties of the mean values δ were voluntarily increased to cover the systematic difference between the triad components (see text).

Fig. 7 shows the results for the Fermi-components $\delta^n(m)$. As one can see, some values have large uncertainties or strong systematic deviations. The reason for the scattering is, most likely, the fine perturbances due to weak lines of CH_4 and CO_2. Not all of these are listed in the HITRAN database, they may sit right underneath strong lines of the triad and are difficult to incorporate in the fit reliably. The most affected is, again, the higher frequency component $20^0 11 \leftarrow 00^0 01$ (orange diamonds in Fig. 7).

The shifting coefficients exhibit a similar behavior for the different components of Fermi triad, although the values for the "middle" $20^0 12 \leftarrow 00^0 01$ band are systematically smaller than for the "lower" and "higher" bands. The lower panel of Fig. 7 illustrates the effect. One can see that most of the compatibility values f for $20^0 12 \leftarrow 00^0 01$ are "pointing down", whereas two other components with $n = 1$ and 3 are "pointing up". We are hesitating to attribute this (rather marginal) difference to the changing extent of Fermi–resonance, but it might well be, since the resonance is very sensitive to the molecular interactions [23], and one component might shift less or more than the other. Like in the case of broadenings, we calculated a weighted average (blue solid line with rectangles in the upper panel of Fig. 7). Since we cannot justify unequivocally that the shifting coefficients are different for the

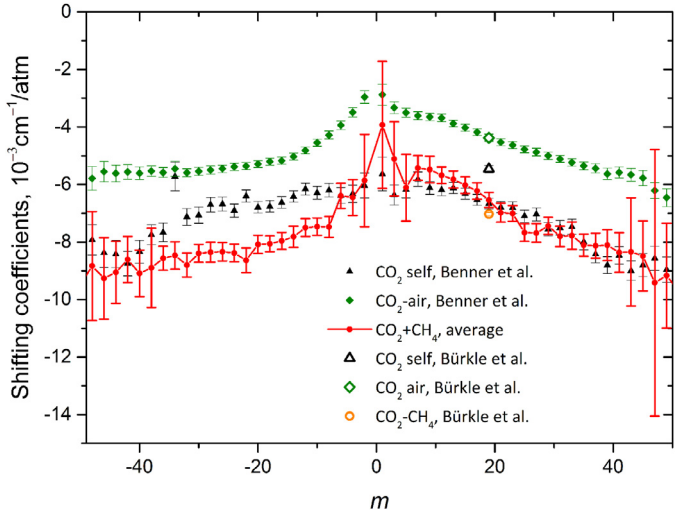

Fig. 8. Shifting of Fermi triad by different buffer gases. CO_2–CH_4 shifting (solid line with filled circles) in an average over all Fermi components. Data for CO_2 self- (filled triangles) and air- shifting (filled diamonds) coefficients for $20^013 \leftarrow 00^001$ is taken from Ref. [21]. Values for R_{18e} for the same band from Ref. 16 are marked by open symbols.

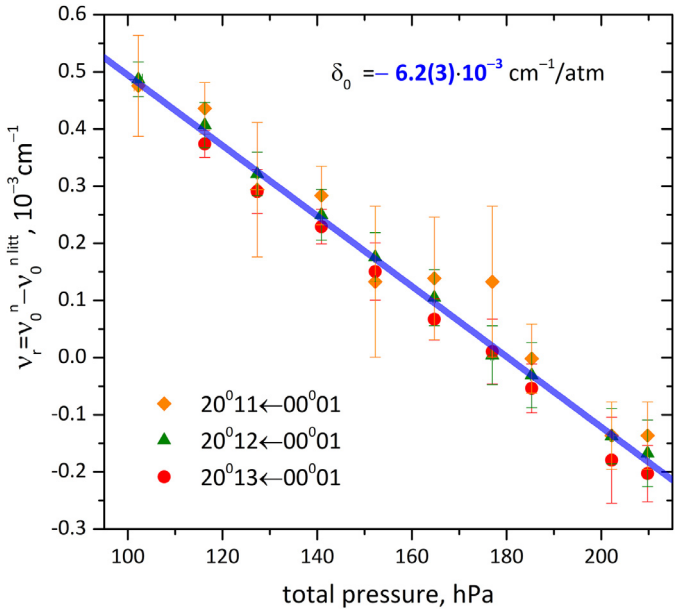

Fig. 9. Reduced vibrational wavenumbers $\nu_r = \nu_0^n - \nu_0^{n\,litt}$ for the Triad components $n = 1 \ldots 3$ as a function of total pressure of CO_2-CH_4 mixture ($\nu_0^{n\,litt}$ are taken from Ref. 11).

Fermi components and rule out an existence of a systematic error, we deliberately increased the uncertainties until the criterion $|f| \leq 1$ is true for most values. In the end, the shifts of the strong lines have the uncertainties of about 4–5%, similar to the uncertainties by Toth [12,15] and self-shifting by Benner [21].

Fig. 8 shows the comparison of self-, air- and CH_4 shifting. One can see that the absolute values for air and CH_4 are very similar (they are coinciding in the R-branch), although the m-dependence for CO_2–CH_4 is closer to self-shifting. There is a good agreement between the results of Bürkle et al. [16] and our measurements, although the compatibility criterion is satisfied for the Fermi-components 1 and 3 but not for the middle component. This might be an indication that there is some systematic error in our measurements. The results from Bürkle et al. [16] agree well with air- and self-shifting from Refs. [12,15] but disagree with the self-shifting from Ref. [21], with f-value is about four.

Additionally, we analyzed the influence of methane collisions on the vibrational wavenumbers of Fermi triad. Vibrational wavenumbers ν_0^n (n labels components of the triad) were determined from the 6th degree polynomial fit of line positions (accounting for the sextic centrifugal constants H). Shifting coefficients δ_0^n were derived from the linear regressions of the obtained vibrational wavenumbers ν_0^n vs. pressure. It turned out that the pure vibrational shifting coefficient is independent on n, so it was possible to combine the data for the components. Reduced wavenumbers $\nu_r = \nu_0^n - \nu_0^{n\,litt}$ are plotted in Fig. 9. $\nu_0^{n\,litt}$ are the vacuum vibrational wavenumbers taken from Ref. [11]. All reduced data points are on the straight line and can be fitted simultaneously. The fit yields the CH_4–shifting coefficient δ_0 of –6.2(3)10^{-3} cm^{-1}/atm. The independence of δ_0 from the triad component works against the idea, that a systematic deviation of the shifting components of the triad is real, but it cannot completely rule it out.

4. Concluding remarks

In the current study we report a large set of data on collisional broadening and shifting coefficients for all three bands of Fermi triad of CO_2 in methane matrix at 296.0(2) K. Most of the data is novel.

The broadening coefficients proved to be the same for all three bands, so the average values were derived with expanded uncertainties (2σ) less than 0.5% for 38 out of 55 reported m-values. A simple empirical expression for the broadening coefficients is obtained. The absolute values of shift coefficients are about ten times smaller than the broadening, and the relative uncertainty is ten times greater (4–5%).

In the future we plan to study how methane absorption changes upon collisions with CO_2, a situation which can occur in biogas processing when the residue of the purification process is monitored.

Acknowledgments

The authors also wish to thank Dr. O. Werhahn for thorough proofreading. The authors acknowledge financial support and collaboration through the European Metrology Programme for Innovation and Research (EMPIR) project 16ENG05-BIOMETHANE. The EMPIR is jointly funded by the EMPIR participating countries within EURAMET and the European Union. R.A. acknowledges a financial support of the Russian Science Foundation (Project 18-13-00050).

References

[1] Mihalcea RM, Baer DS, Hanson RK. Diode laser sensor for measurements of CO, CO_2, and CH_4 in combustion flows. Appl Opt 1997;36:8745–52. doi:10.1364/AO.36.008745.
[2] Kim YJ, Yong YSN, Kang T. Study on a numerical model and PSA (pressure swing adsorption) process experiment for CH_4/CO_2 separation from biogas. Energy 2015;91:732–41. doi:10.1016/j.energy.2015.08.086.
[3] Biomethane, EMPIR project: http://empir.npl.co.uk/biomethane [accessed Accessed 2 July 2019].
[4] Bradford MCJ, Vannice MA. CO_2 reforming of CH_4. Catal Rev 1999;41:1–42. doi:10.1081/CR-100101948.
[5] DeQ Vu, Koros WJ, Miller SJ. High pressure CO_2/CH_4 separation using carbon molecular sieve hollow fiber membranes. Ind Eng Chem Res 2002;41:367–80. doi:10.1021/ie010119w.
[6] Nwaboh JA, Werhahn O, Ortwein P, et al. Laser-spectrometric gas analysis: CO_2-TDLAS at 2 μm, measurement. Sci and Technol 2013;24:015202. doi:10.1088/0957-0233/24/1/015202.
[7] Nwaboh JA, Pratzler S, Werhahn O, et al. Tunable diode laser absorption spectroscopy sensor for calibration free humidity measurements in pure methane and low CO_2 natural gas. Appl Spectrosc 2017;71:888–900. doi:10.1177/0003702816658672.

[8] Domanskaya AV, Li G, Tran H, Gisi M, Ebert V. Collision-induced line parameters for the (2←0) overtone band of HCl (1.76 μm) in binary mixtures with H_2 and CH_4. JQSRT 2017;199:71–6. doi:10.1016/j.jqsrt.2017.05.0150022-4073.
[9] Nwaboh JA, Domanskaya AV, Qu Z, Werhahn O, Ebert V. Laser-based hydrogen chloride measurements for biogas and biomethane applications. The 25th international conference on high resolution molecular spectroscopy, P2.35, abstract book: page 276, 3-7.09, Bilbao; 2018.
[10] Gordon IE, Rothman LS, Hill C, Kochanov RV, Tan Y, Bernath PF, Birk M, Boudon V, Campargue A, Chance KV, Drouin BJ, Flaud J-M, Gamache RR, Hodges JT, Jacquemart D, Perevalov VI, Perrin A, Shine KP, Smith M-AH, Tennyson J, Toon GC, Tran H, Tyuterev VG, Barbe A, Császár AG, Devi VM, Furtenbacher T, Harrison JJ, Hartmann J-M, Jolly A, Johnson TJ, Karman T, Kleiner I, Kyuberis AA, Loos J, Lyulin OM, Massie ST, Mikhailenko SN, Moazzen-Ahmadi N, Müller HSP, Naumenko OV, Nikitin AV, Polyansky OL, Rey M, Rotger M, Sharpe SW, Sung K, Starikova E, Tashkun SA, Vander Auwera J, Wagner G, Wilzewski J, Wcisło P, Yu S, Zak EJ. The HITRAN2016 molecular spectroscopic database. JQSRT 2017;203:3–69. doi:10.1016/j.jqsrt.2017.06.038.
[11] Miller CE, Brown LR. Near infrared spectroscopy of carbon dioxide. $^{16}O\ ^{12}C^{16}O$ line positions. J Mol Spectrosc 2003;228:329–54. doi:10.1016/j.jms.2003.11.001.
[12] Toth RA, Brown LR, Miller CE, Devi VM, Benner DC. Self-broadened widths and shifts of $^{12}C^{16}O_2$: 4750–7000 cm^{-1}. J Mol Spectrosc 2006;239:243–71. doi:10.1016/j.jms.2006.08.003.
[13] Gamache RR, Lamouroux J. The vibrational dependence of half-widths of CO_2 transitions broadened by N_2, O_2, air and CO_2. JQSRT 2013;117:93–103. doi:10.1016/j.jqsrt.2012.10.028.
[14] Gamache RR, Lamouroux J, Blot-Lafon V, Lopes E. An intercomparison of measured pressure-broadening, pressure shifting parameters of carbon dioxide and their temperature dependence. JQSRT 2014;135:30–43. doi:10.1016/j.jqsrt.2013.11.001.
[15] Toth RA, Miller CE, Devi VM, Benner DC, Brown LR. Air-broadened halfwidths and pressure shifts of $^{12}C^{16}O_2$ bands: 4750–7000 cm^{-1}. J Mol Spectrosc 2007;243:133–57. doi:10.1016/j.jms.2007.09.005.
[16] Bürkle S, Walter N, Wagner S. Laser-based measurements of pressure broadening and pressure shift coefficients of combustion-relevant absorption lines in the near infrared region. Appl Phys B 2018;124:121. doi:10.1007/s00340-018-6993-y.
[17] Central spectroscopic facility organised in the frame of the EUMETRISPEC project. http://www.eumetrispec.org/ [accessed Accessed 2 July 2019].
[18] Li G, Asfin RE, Domanskaya AV, Ebert V. He-broadening and shifting coefficients of HCl lines in the (1←0) and (2←0) infrared transitions. Mol Phys 2018;116:3495–502. doi:10.1080/00268976.2018.1457805.
[19] York D, Evensen NM. Unified equations for the slope, intercept, and standard error of the best straight line. Am J Phys 2004;72:367–75. doi:10.1119/1.1632486.
[20] Joint Committee for Guides in Metrology, BIPM. International vocabulary of metrology. https://www.bipm.org/en/publications/guides/vim.html [accessed Accessed 2 July 2019].
[21] Benner DC, Devi VM, Sung K, et al. Line parameters including temperature dependences of air- and self-broadened line shapes of $^{12}C^{16}O_2$: 2.06-μm region. J Mol Spectrosc 2016;326:21–47. doi:10.1016/j.jms.2016.02.012.
[22] Buckingham AD. A theory of frequency, intensity and band-width changes due to solvents in infra-red spectroscopy. Proc R Soc Lond 1960;255A:32–8. doi:10.1098/rspa.1960.0046.
[23] Birnbaum G. Phenomena induced by intermolecular interactions. NATO ASI series, series B: physics, 127. New York and London: Plenum Press; 1985. doi:10.1007/978-1-4613-2511-1.